

Slow-light: Fascinating physics or potential applications?

Slow light pulse propagation in dispersive media

Torben Roland Nielsen *, Jesper Mørk, Andrei V. Lavrinenko

DTU Fotonik – Department of Photonics Engineering, Technical University of Denmark, Ørstedsgade 343, DK-2800 Kgs. Lyngby, Denmark

Available online 31 December 2009

Abstract

We present a theoretical and numerical analysis of pulse propagation in a semiconductor photonic crystal waveguide with embedded quantum dots in a regime where the pulse is subjected to both waveguide and material dispersion. The group index and the transmission are investigated by finite-difference-time-domain Maxwell–Bloch simulations and compared to analytic results. For long pulses the group index (transmission) for the combined system is significantly enhanced (reduced) relative to slow light based on purely material or waveguide dispersion. Shorter pulses are strongly distorted and depending on parameters broadening or break-up of the pulse may be observed. The transition from linear to nonlinear pulse propagation is quantified in terms of the spectral width of the pulse. **To cite this article: T.R. Nielsen et al., C. R. Physique 10 (2009).**

© 2009 Académie des sciences. Published by Elsevier Masson SAS. All rights reserved.

Résumé

Propagation lente d'impulsions lumineuses dans les milieux dispersifs. Nous présentons une analyse théorique et numérique de la propagation d'impulsions dans un guide d'ondes à cristaux photoniques à semi-conducteurs à boîtes quantiques dans un régime où l'impulsion est soumise simultanément à la dispersion guide et à la dispersion matériau. L'indice de groupe et la transmission sont analysés par des simulations numériques de type FDTD (Finite Difference Time Domain) des équations de Maxwell–Bloch et comparées aux résultats analytiques. Pour des impulsions longues, l'indice de groupe (transmission) pour le système combiné est augmenté (diminué) de manière significative par rapport au cas d'une dispersion purement guide ou matériau. Les impulsions courtes sont fortement déformées et en fonction des paramètres d'élargissement un éclatement de l'impulsion peut être observé. La transition du régime de propagation linéaire au cas non-linéaire est quantifiée en terme de largeur spectrale d'impulsion. **Pour citer cet article : T.R. Nielsen et al., C. R. Physique 10 (2009).**

© 2009 Académie des sciences. Published by Elsevier Masson SAS. All rights reserved.

Keywords: Slow light; Photonic crystals; Quantum dots; Electromagnetically induced transparency

Mots-clés : Ralentissement de la lumière ; Cristaux photoniques ; Boîtes quantiques ; Transparence induite par électromagnétisme

1. Introduction

Slow light phenomena have attracted much attention over the last decade due the possible applications in optical signal processing [1]. Optical memory, delay lines, switches, and phase-array antenna are among the main targeted device applications currently under study. Several physical mechanisms have been proposed and used to realize an

* Corresponding author.

E-mail address: trol@fotonik.dtu.dk (T.R. Nielsen).

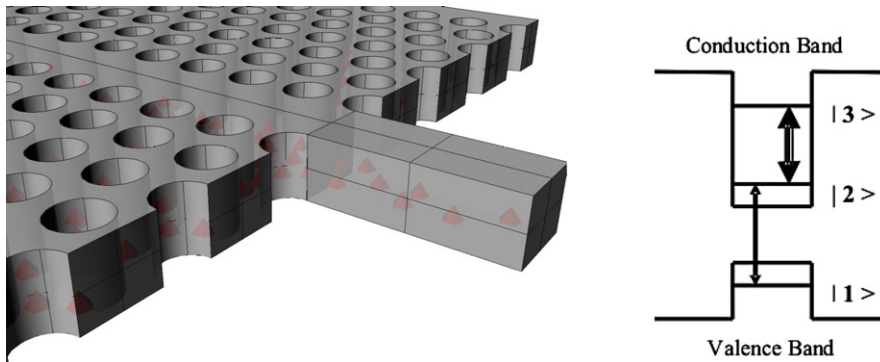


Fig. 1. Left: Photonic crystal waveguide with quantum dots. Right: Energy level scheme for quantum dots.

all-optical buffer. In general, they can be divided into two categories – one where the device has a nontrivial waveguide dispersion property and a second where the material guiding the optical signal exhibits a nontrivial dispersion. A photonic crystal waveguide (PhC WG) is an example of a system with a nontrivial waveguide dispersion resulting in slow light propagation in the vicinity of the band edge [2], while slow light based on material dispersion is known from experiments on atomic vapor gasses by using electromagnetically induced transparency (EIT) [3]. Since the dispersion properties of slab PhC WGs are predetermined by the PhC structure and the bulk material properties, variable slow down factors cannot easily be obtained for fixed frequencies. However, introducing optical nonlinearities into the PhC are predicted to have significant technological impact on signal processing [4]. Slow light based on semiconductor quantum dots (QDs) EIT systems, on the other hand, sets rather strict requirements to the dephasing rates, dipole moments, QD densities and uniformity of the QD ensemble [5]. So far most studies of pulse propagation have focused on engineering separately the material or the waveguide dispersion. Little has been done to understand the combined effects of material and waveguide dispersion. A full vectorial finite-difference-time-domain (FDTD) analysis of the electromagnetic fields is needed in order to give a proper description of pulse propagation in these strongly diffractive PhC structures. In this article we show that by combining both waveguide and material dispersion the slow light effect can be drastically different compared to the individual subsystems.

As an example we consider a W1 PhC WG slab geometry with QDs embedded in the structure, see Fig. 1. We examine an EIT QD slow light configuration which is excited in the cascade arrangement, i.e. a weak signal beam is resonant with the QD electron-hole ground state transition, while a strong pump beam is applied between the QD electron ground state and a third excited electron state. The QD electron-hole ground state transition is in the vicinity of the PhC WG band edge. The pump beam creates a spectral hole at electron-hole ground state transition in the QD absorption background, which by the Kramers–Krönig relation implies a change in real part of the dielectric function. In this way the QDs can be used to alter the optical susceptibility of the dielectric host. We investigate the influence of the strength of the pump pulse and the temporal width of the signal beam with respect to the group index and the transmission of the signal beam. The paper is organized as follows. In Section 2 the slow down properties of a QD ensemble in bulk dielectric host are investigated. In Section 3 analytic scaling laws for the group index and transmission of PhC WGs with material dispersion are investigated, and compared with FDTD simulation in Section 4. The paper is concluded in Section 5.

2. Slow light based on material dispersion

We consider an ensemble of QDs, which is excited in the EIT cascade configuration [5]. If we just focus on the three levels coupled by the optical fields, and neglect any interaction with energetic closely lying confined QD or delocalized states, the corresponding QD energy level scheme is shown in the right part of Fig. 1. The transition between level $|2\rangle$ and level $|3\rangle$ is dipole disallowed, while the two resulting transitions are dipole allowed.

The optical linear response of the system to an external weak perturbation (the signal beam) is evaluated according to a semiclassical theory, where the time-dependent microscopic polarization of the QDs induces a change in the macroscopic dielectric function of the medium. The QD carrier dynamics is described through the elements of the density matrix and are evolved in time according to the Liouville equation

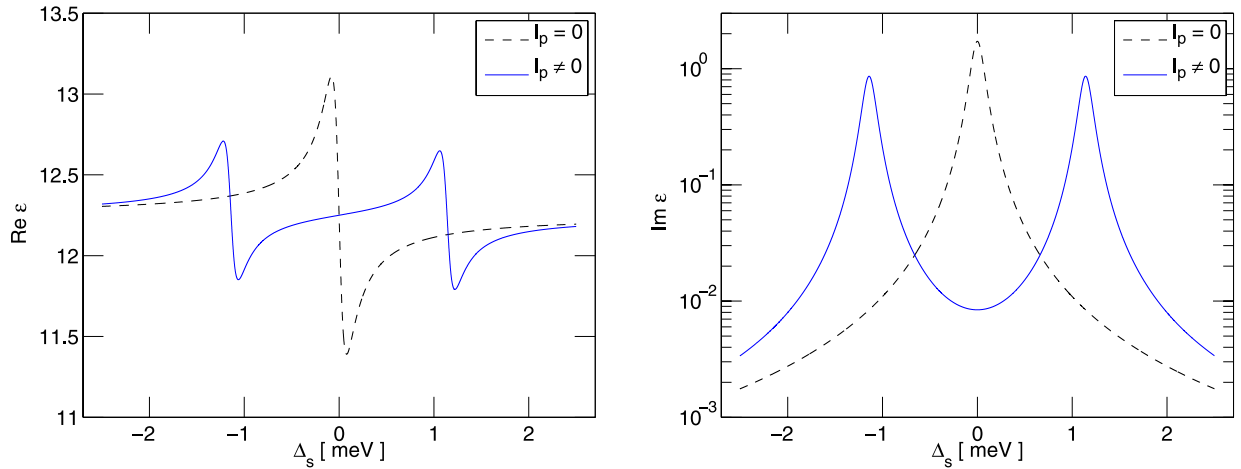


Fig. 2. Real and imaginary parts of the dielectric function with (solid line) and without (dashed line) coupling field present.

$$\frac{\partial}{\partial t} \rho = \frac{1}{i\hbar} [H, \rho] - \frac{1}{2} \{\gamma, \rho\} \tag{1}$$

where H is the Hamiltonian $H = H_0 + H_d$ with the non-interacting part H_0 and the dipole interaction H_d while γ describes the dephasing.

The first-order optical susceptibility seen by the signal beam is evaluated as follows. The system is driven with a monochromatic continuous wave (CW) pump and signal beams of Rabi energy $\hbar\Omega_{p,s} = \mu_{p,s}E_{p,s}$ with $\mu_{p,s}$ being the correspondent dipole moments and $E_{p,s}$ the amplitudes of the electric field. It is assumed that the pump beam is much stronger than the signal beam, i.e., $\Omega_p \gg \Omega_s$. Then in steady state the relative macroscopic dielectric constant around the signal frequency is given by

$$\langle \omega \rangle = \left[\varepsilon_b + i \frac{\Gamma |\mu_{21}|^2}{V \varepsilon_0} \frac{(f_1 - f_2)}{\tilde{\gamma}_{21} [1 + |\Omega_p|^2 / (\tilde{\gamma}_{21} \tilde{\gamma}_{32})]} \right] \tag{2}$$

where $\tilde{\gamma}_{21} = \gamma_{21} + i\Delta_s$ and $\tilde{\gamma}_{31} = \gamma_{31} + i(\Delta_s + \Delta_p)$ with the detunings $\Delta_s = \omega_{21} - \omega_s$ and $\Delta_p = \omega_{32} - \omega_p$. The population of first and second level is denoted f_1 and f_2 . The bulk dielectric background constant is denoted ε_b , Γ is the optical confinement factor, and V is the volume of a single QD.

In deriving Eq. (2), the inhomogeneity of the QD ensemble is neglected for illustrative purposes. For the results presented here, we use typically InGaAs QD parameters as given in Ref. [6]. In contrast to EIT in atomic based systems, the dephasing rate for the optically uncoupled coherence in QD based EIT systems can usually not be neglected, as all involved QD states interact equally well with the surrounding environment which in turn caused the loss of coherence; mainly through carrier–carrier and carrier–phonon interaction. This is a general problem one faces when dealing with semiconductor systems. For this reason we choose the two dephasing rates to be of the same order of magnitude, $\gamma_{21} = \gamma_{31} = \gamma$.

The real and imaginary parts of the dielectric constant, Eq. (2), are shown in Fig. 2 as a function of the signal frequency with and without the pump beam present. When the pump beam is turn off, the system reduces to an ensemble of two-level emitters with an absorption line at zero signal detuning and a width of γ . By the Kramers–Krönig relation a change in the absorption line implies a change in the real part of the dielectric function. When a resonant pump beam is turn on the absorption line is split, and the QD ensemble becomes transparent at zero signal detuning. The separation of the two resonance peaks in the absorption spectrum is Ω_p and is sometimes also discussed in terms of the dressed states of the system, brought about by the strong pump laser field.

The slow down factor S is defined as the speed of light in free space relative to the group velocity $S = c_0/v_g$, thus for purely material induced dispersion the slow down factor reads

$$S = n + \omega \frac{\partial}{\partial \omega} n = \text{Re} \sqrt{\varepsilon} + \omega \frac{\partial}{\partial \omega} \text{Re} \sqrt{\varepsilon} \tag{3}$$

which by using Eq. (2) at zero detunings can be reduced to

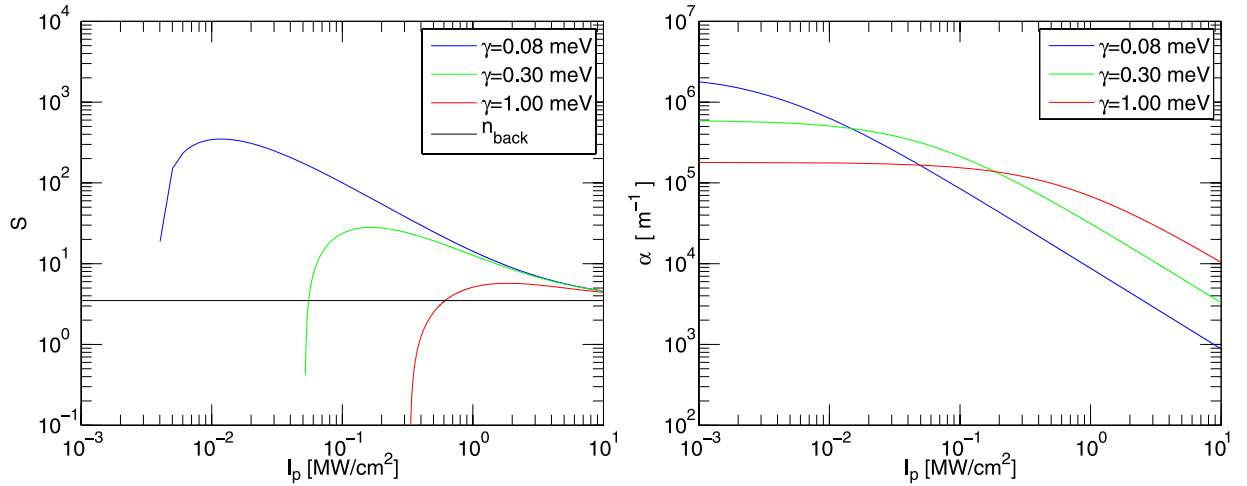


Fig. 3. Left: Slow down factor as a function of pump power density. Right: Absorption coefficient as a function of pump power density.

$$S = \left[\frac{\varepsilon_b + \sqrt{\varepsilon_b^2 + \varepsilon_{res}^2}}{2} \right]^{1/2} \times \left[1 + \frac{\hbar\omega_s}{2\sqrt{\varepsilon_b^2 + \varepsilon_{res}^2}} \frac{U_{21}(\Omega_p^2 - \gamma_{31}^2)}{\hbar^2(\gamma_{21}\gamma_{31} + \Omega_p^2)} \right] \quad (4)$$

where $U_{21} = \Gamma|\mu_{21}|^2(f_1 - f_2)/(V\varepsilon_0)$ and $\varepsilon_{res} = U_{21}/[\hbar(\gamma_{21} + \Omega_p\gamma_{31})]$.

The slow down factor S based on Eq. (4) is plotted in Fig. 3 as a function of the pump power density, $I_p = c_0\varepsilon_0n_bE_p^2$. The three different dephasing rates shown in Fig. 3 correspond to three different temperature regimes, ranging from sub-cryogenic to room temperatures [5]. The slow down factor is reduced for increasing dephasing rates, as the mechanism behind EIT, which relies on retaining high degree of quantum mechanical coherence between the states is reduced for large dephasing rates. The dependency of the slow down factor on the pump power density is to be understood as follows. At small intensities the pump field is not strong enough to split the levels and the signal beam is absorbed. At high pump power densities, the splitting of the levels is large, resulting in almost no absorption and a small slope of the real part of ε at the signal frequency. Hence, the slow down factor reaches the bulk value of n_{bac} . In-between these two extremes, there exists an optimum for the slow down factor. In Fig. 3 we also plot the absorption coefficient $\alpha = 2\omega/c_0 \text{Im} \sqrt{\varepsilon(\omega)}$ as a function of the pump power density. At high pump power densities where the Rabi splitting is much larger than the dephasing the systems become effectively transparent. As the pump power is decreased the absorption increases and reaches a plateau given by the ensemble of two-level emitters. Thus, the high slow down factors are associated with high absorption coefficients.

3. Slow light based on waveguide and material dispersion

Using first-order perturbation theory the group index in a system based on both material and waveguide dispersion may be evaluated from the individual subsystems [6]

$$n_g = (1 - E_d)n_g^{PhC} + \kappa S \quad (5)$$

where $\kappa = E_d n_g^{PhC}/n_b$ and E_d is the filling factor giving the electric energy inside the QD region. For a fixed PhC WG group index n_g^{PhC} the total group index, n_g , scales linear with the dispersive group index, or the so called slow down factor S . Similar linear scaling may also be obtained for fixed dispersion group index and variable PhC WG group index. The transmission can be evaluated from first-order perturbation theory as shown in Ref. [7]

$$T = \exp\{-\kappa\alpha L\} \quad (6)$$

where $T = I_{in}/I_{out}$ and L is the length of the PhC WG. For a fixed PhC WG group index the transmission has a power dependency of the material based absorption coefficient. Similar scaling may also be obtained for fixed absorption coefficient and variable PhC WG group index. Thus, by using Eqs. (5) and (6) and the results for material dispersive based slow light a maximum performance of a device relying on waveguide and material dispersion can be estimated.

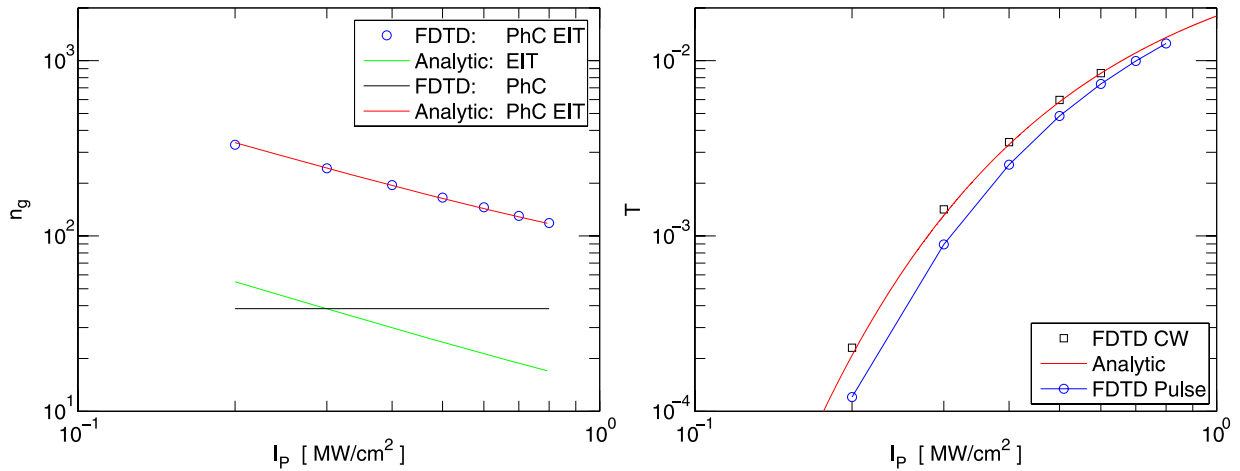


Fig. 4. Left: Group index as a function of the pump power density. Right: Corresponding transmission for the PhC WG EIT system as a function of the pump power density.

4. Pulse propagation in dispersive media

To study pulse propagation in systems with both waveguide and QD material dispersion, we use a fully self-consistent FDTD Maxwell–Bloch model, thereby treating the electromagnetic fields and the microscopic polarization on an equal footing. The light–matter interaction is analyzed within the dipole approximation. When implemented on a FDTD mesh the Liouville equation is solved at every grid point. Together with Amperes law for propagating the magnetic field strength, we solve numerically the set of equations without any further approximations. See Ref. [6] for technical details and device parameters. The signal beam which is resonant with electron–hole ground state transition and TE polarized, while the CW pump beam is resonant with the electron–electron transition, polarized perpendicular to the signal beam and propagates in the direction perpendicular to the PhC membrane. The group index is determined by a time of flight method giving the delay time between the peak of the pulse just before the entrance and just after the exit of the PhC WG. The incoming signal field has a temporal Gaussian envelope. For the numerical results related to the group index, we consider signal pulses whose spectral width is well located within the two EIT absorption peaks, which arise due to the dressing of the system by the pump beam, see Fig. 2. For these parameters the pulse propagates fairly undistorted through the waveguide, with only a small temporal widening of the pulse. Thus a time delay between the in- and output pulses can be attributed and a group index can be extracted.

In Fig. 4 we plot the group index for pulses propagating through a passive PhC WG, ridge waveguide (RWG) embedded with QDs, and the QD PhC WG system as a function of the applied pump power density I_p . The temporal full-width-half-maximum (FWHM) of the signal field is fixed to $\tau_s = 9.6$ ps. The passive PhC WG group index is independent of the pump power density and therefore constant for all power densities. The group index for the RWG EIT system is determined from the analytic model, Eq. (4), and decreases with increasing pump power density. As the pump power density is lowered the group index increases dramatically as also discussed in Section 2. The group index for the combined system, which explores both material and waveguide dispersion, increases as the pump power is decreased, thus showing the same dependency as the RWG EIT system. It is observed that the group index is increased dramatically for the combined system compared to the individual subsystems. Notice that a small change in the pump power density gives a large change in group index for the combined system compared to the RWG EIT system. In Fig. 4 we have also plotted the prediction of Eq. (5). The electric energy in side the QD region is evaluated from the numerical simulations. From our calculations we obtain $n_g^{PhC} = 38.5$ and $E_d = 0.53$. We observe good agreement between numerical simulations and theory. Thus, by combining both material and waveguide dispersion it is possible to enhance the group index as well as obtaining a variable and controllable group index in an ultra small WG structure.

In Fig. 4 we have also plotted the corresponding transmission for the PhC WG EIT system as a function of the pump power density for the pulsed FDTD, CW FDTD, and for the analytic results given by Eq. (6). Here the transmission is defined as $T = E_{out}^2/E_{in}^2$ and the analytic result in Eq. (6) has been scaled with the transmission coefficient for the

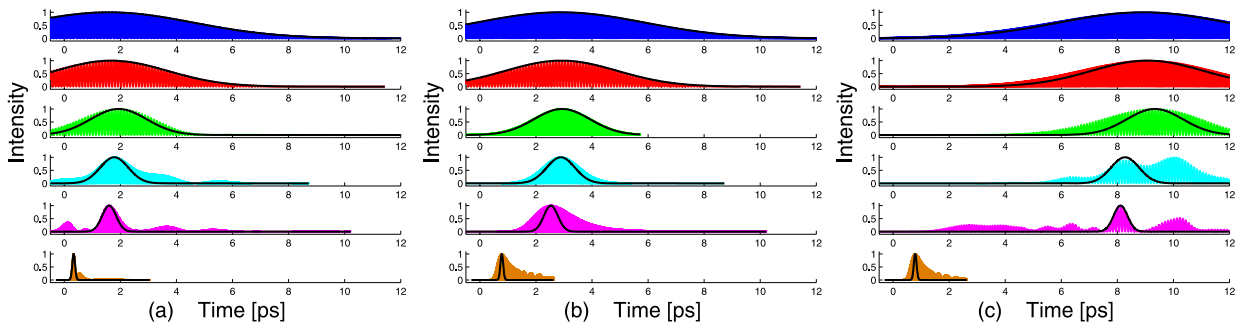


Fig. 5. Normalized output signal intensity for the RWG EIT system (a), PhC WG system (b), and PhC WG EIT system (c). The incoming signal field has a temporal FWHM of $\tau_s = \{9.6, 6.4, 3.2, 1.6, 0.8, 0.16\}$ ps (blue, red, green, cyan, magenta, brown). The solid black line corresponds to normalized envelope of the incoming signal intensity shifted from its maximum at Time = 0 to coincide with the peak of the output signal beam.

passive PhC WG to account for in- and out-coupling losses. As the pump power density is increased the transmission is increased as the absorption coefficient α drops of with higher pump power as shown in Fig. 3. We notice good agreement between the CW FDTD and the analytic results. Comparing the pulsed FDTD results to the analytic, we see a significant difference in the transmission at low pump powers. In this regime the absorption changes rapidly over the spectral width of the signal pulse which leads to an effective larger absorption coefficient. This effect is illustrated by Fig. 2, where the imaginary part of the dielectric constant is plotted for $I_p = 0$ and 0.8 MW/cm^2 . As the pump power is decreased the splitting of the absorption line is also decreased. Since the spectral width of the signal field is fixed, the overall effective absorption coefficient is larger than the monochromatic result of Eq. (6) giving a larger discrepancy between the pulsed FDTD and analytic results at low pump power densities.

The above results showed good agreement between the analytic results and the numerical simulations for temporal long signal fields and high pump power densities, while at low pump power densities some deviation between the numerical and analytic results for the transmission was observed. In the following we investigate the influence of the temporal width of the signal beam. As a typical example we fix the pump power density to $I_p = 0.8 \text{ MW/cm}^2$ and vary the temporal width of the signal field. In Fig. 5 we plot the normalized output signal intensity for the three systems: (a) RWG EIT, (b) PhC WG, and (c) PhC WG EIT for different temporal widths of the incoming signal field. Let $\Delta\omega_\tau$ denote the spectral FWHM of the incoming signal field. Then, in terms of the pump Rabi frequency Ω_p the spectral width is varied from $\Delta\omega_\tau/\Omega_p = \{0.1, 0.16, 0.32, 0.65, 1.30, 6.47\}$ ranging from temporal long to short pulses. Temporal long pulses propagate undistorted through the WG and group index can easily be assigned to the system. The top parts of Fig. 5(a), (b), and (c) were used to evaluate the group index and transmissions in Fig. 4. As the spectral width of the incoming signal field is increased, the output signal field starts to be distorted resulting in temporal broadened or even pulse break-up. This is true for all the systems under study as they all have reminisces of dispersion. The exact amount of distortion is dependent on the specific system and must in general be determined by a detailed study. For spectral width on the order of the Rabi frequency, such as e.g. $\Delta\omega_\tau/\Omega_p = 1.30$, the output signal has both fast and slow components for the RWG EIT system, while for the PhC WG system the output signal just broadened as the characteristic EIT pump Rabi frequency is not present in the passive PhC WG system. For the PhC WG EIT system the pulse is completely distorted. From the figures it is observed that spectrally narrow pulses with a spectral width on the order of $\Delta\omega_\tau/\Omega_p = 0.1$ can be described by linear pulse propagation, while for short temporal pulses the system is nonlinear.

In order to quantify these observations and to measure temporal broadening we plot in Fig. 6 the delay time and the square root of the temporal variance of the output signal intensity. The average delay time is defined as

$$t_{av} = \frac{\int dt t |E(t)|^2}{\int dt |E(t)|^2}$$

while the square root of the temporal variance is defined as

$$\sigma = \sqrt{\langle t^2 \rangle - t_{av}^2}$$

where

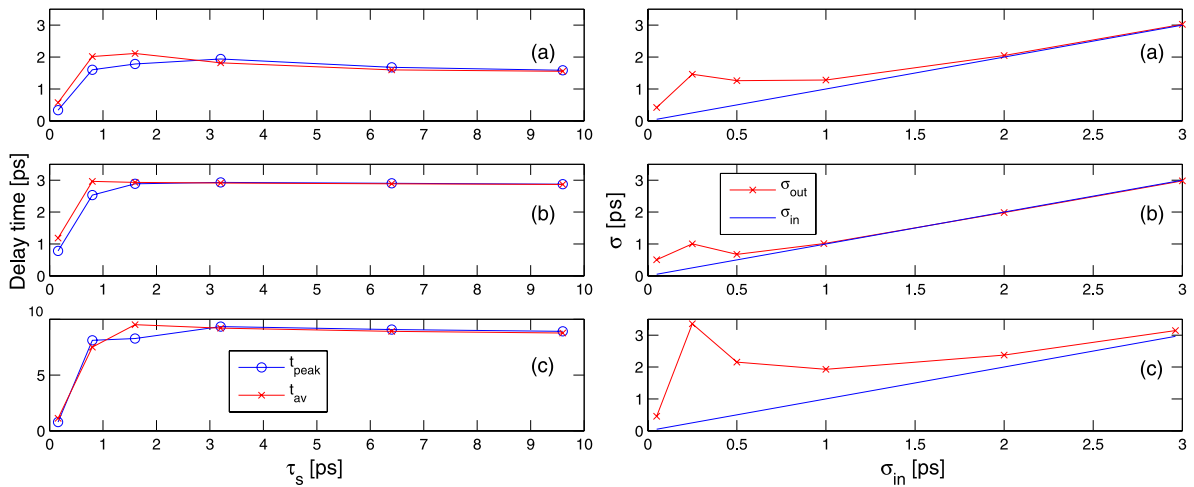


Fig. 6. Left: Delay time as a function of the FWHM of the incoming signal field τ_s . Right: Square root of the variance of the output signal intensity as a function of the square root of incoming intensity temporal width. The top row corresponds to the RWG EIT system (a), the middle row is for the PhC WG system (b), while the bottom row is for the PhC WG EIT system (c).

$$\langle t^2 \rangle = \frac{\int dt t^2 |E(t)|^2}{\int dt |E(t)|^2}$$

For long pulses the mean delay time t_{av} and the peak time t_{peak} are almost equal, which they should be if the symmetric input signal propagates undistorted through the system. In general the peak and mean value agrees well for spectral width up to $\Delta\omega_\tau/\Omega_p = 0.32$. In Fig. 6 we have also plotted the square root of temporal variance of the signal field as a function of the square root of the temporal variance of the incoming intensity for the RWG EIT, PhC WG, and PhC WG EIT systems. For the PhC WG EIT system a spectral width up to $\Delta\omega_\tau/\Omega_p = 0.16$ the σ_{out}/σ_{in} ratio is below 1.2, and for shorter temporal pulses the output pulse is broaden significantly. Thus, even though a given pulse width is acceptable for distortion free pulse propagation for RWG EIT or PhC WG systems, pulse propagation in the combined system might still be significantly distorted as seen by the example of $\Delta\omega_\tau/\Omega_p = 0.32$, where only the RWG EIT gives rise to a small distortion, but for the combined system the distortion is larger. Thus, if the spectral width of the incoming field is below or around $\Delta\omega_\tau/\Omega_p = 0.1$ pulse propagation is linear, while above this limit this is nonlinear.

5. Conclusion

In conclusion, we have investigated slow light pulse propagation in a semiconductor photonic crystal waveguide with embedded quantum dots in a regime where the pulse is subjected to both waveguide and material dispersion. For a fixed PhC WG design, operating at a fixed frequency, the total group index can be varied by using an external pump field. The group index may thus be enhanced compared to the individual subsystem, but at the cost of a reduction in the transmission. For pulsed systems the transmission is furthermore reduced due to larger effective absorption compared to the CW case. A quantitative study shows that the combined system can be described by linear pulse propagation, for spectrally narrow pulses below 10% of the pump field Rabi frequency. At shorter temporal pulses the signal is distorted, giving rise to temporal bordering or eventual pulse break up. In this regime, the system is nonlinear and cannot be described by linear pulse propagation.

References

- [1] P.C. Ku, C.J. Chang-Hasnain, S.L. Chuang, J. Phys. D 40 (2007) R93–R107.
- [2] A. Vlasov, M. O’Boyle, H.F. Hamann, S.J. McNab, Nature 438 (2005) 65–69.
- [3] L.V. Hau, S.E. Harris, Z. Dutton, C.H. Behroozi, Nature 397 (1999) 594–598.
- [4] M. Soljacic, J.D. Joannopoulos, Nat. Mater. 3 (2004) 211–219.
- [5] C.J. Chang-Hasnain, P.C. Ku, J. Kim, S.H. Chuang, Proc. IEEE 9 (2003) 1884–1897.
- [6] T.R. Nielsen, A. Lavrinenko, J. Mørk, Appl. Phys. Lett. 94 (2009) 113111.
- [7] N.A. Mortensen, S. Xiao, Appl. Phys. Lett. 90 (2007) 141108.